Scientia Iranica, Vol. 10, No. 2, pp 194–202

SCIENTIA
IRANICA

An Actuator-Level Robust Joint Torque Control of Robot with Harmonic Drive Transmission

M.M. Moghaddam* and A.A. Goldenberg[1]

Motion and torque control of flexible joint robots is difficult, due to the inherent characteristics of such systems. The joint flexibility may generate resonant frequencies within the range of control bandwidth that may destabilize the system. The joint flexibility should be considered in motion control of high performance robots. This paper presents a new $\mathcal{H}_\infty-$ based torque control design method for flexible joint robots. First, a nominal torque transfer function of the joint is identified from input-output experimental tests. Second, by varying the input signal amplitude, a set of models describing the effect of nonlinearities in the system is extracted. The difference between this set and the nominal transfer function defines the uncertainty bounds for control design purposes. Third, an $\mathcal{H}_\infty-$ based torque control law is designed to minimize the ∞-norm of the torque transfer function. Finally, the effectiveness of the proposed torque control design method is experimentally verified on the IRIS-facility (a versatile, modular and reconfigurable prototype robot developed at the Robotics and Automation Laboratory of the University of Toronto).

INTRODUCTION

Motion control of flexible joint robots has been the subject of many research investigations over the past decade. It is an interesting and challenging problem as well as useful, because most robots exhibit some degree of joint flexibility. It is a challenging issue since the joint flexibility introduces undesired degrees of freedom at the robot joints, making the control of such systems a difficult task. The sources of joint flexibility may be gears, belts, chains, torsional shafts, torque transducers or harmonic drives [1,2]. Problems of robot manipulation and joint flexibility were addressed in [3]. In the literature, different techniques have been proposed to deal with related modeling and control issues. In general, control schemes suitable for flexible joint robots can be categorized as: Simple PID, feedback linearization, integral manifold, singular perturbation, passivity approach, torque feedback and adaptive control designs. A simple PD controller for robots with flexible joints was introduced in [4]. A singular perturbation technique to control flexible joint robots was proposed in [5]. In [6] an adaptive controller, based on integral manifold and singular perturbation techniques, was constructed, assuming high joint flexibility. An adaptive control law for flexible joint robot control was introduced in [7]. The effect of joint flexibility on robot motion control, based on joint torque feedback, was presented in [8]. A robust adaptive control of flexible joint robots with joint torque feedback was proposed in [9].

In this paper, the torque control problem of a flexible joint robot is considered. A nominal input-output torque transfer function is derived from experimental tests. Furthermore, by changing the input command amplitude, a set of models that describe the effect of nonlinearities is identified. The difference between this set and the nominal model is then incorporated into the control design procedure through the use of uncertainty bounds and weighting functions. The role of the weighting functions is to model the variation between the real and nominal system model. Furthermore, the effects of sensor noise, actuator-saturation limit and unmodeled high-frequency dynamics are considered through another set of weighting functions. The robustness and performance requirements of the closed-loop system are traded off through modifications of the weighting functions [10]. Finally, the theoretical design is experimentally validated on the IRIS-facility setup.

The paper is organized as follows. First, the prob-

*. *Corresponding Author, Department of Mechanical Engineering, University of Tarbiat Modarres, Tehran, I.R. Iran.*

1. *Robotics and Automation Laboratory, Department of Mechanical Engineering, University of Toronto, Canada.*

lem formulation is presented. Then, the experimental identification of the nominal torque transfer function is discussed and the determination of uncertainty bounds is presented. After that, the proposed actuator-level torque control design and the experimental setup are introduced. Then, the experimental evaluation of the proposed control law is investigated and finally, the results are summarized .

PROBLEM FORMULATION

To include actuator dynamics into robust control design of flexible joint robots the recursive or backstepping design method [11] is followed. In doing so, one starts with the model of a flexible joint robot and derives its error dynamics model. Furthermore, using $\mathcal{H}_\infty-$ design method, a joint torque control design is proposed to guarantee the stability and convergence of the error dynamics model [12].

The model of an n-DOF flexible joint robot with HD transmission can be written as follows [13,14]:

$$M(q_c)\ddot{q}_c + N(q_c, \dot{q}_c) = \frac{r+1}{r}\tau_h, \tag{1}$$

$$J_{mw}\ddot{q}_m + B_{mw}(q_m, \dot{q}_m, q_c) + (B^+_{mw}, B^-_{mw})Sgn(\dot{q}_m) + \frac{1}{r}\tau_h = \tau_m, \tag{2}$$

where q_c and q_m are the $n \times 1$ vectors of shaft displacement on the joint side and actuator side, respectively, $M(q_c)$ is a $n \times n$ link inertia matrix, $N(q_c, \dot{q}_c)$ is a $n \times 1$ vector of centrifugal, gravity, and Coriolis (generalized) forces; τ_h is the torque sensor output located at the link side, r is the harmonic drive gear ratio, J_m is the $n \times n$ diagonal matrix of actuator inertia, B_{mw} is a $n \times 1$ vector of damping and (B^+_{mw}, B^-_{mw}) are friction terms associated with the actuator and H.D. bearings. τ_m is the $n \times 1$ vector of control torque input.

The first step in the proposed design method is the formulation of the error dynamics. Let the link position error be defined as:

$$e = q^d_c - q_c, \tag{3}$$

where q_c is the $n \times 1$ link position and q^d_c the $n \times 1$ desired link position vector, respectively. It is assumed that q^d_c and its derivatives up to the third order are bounded. Now, the rigid-body dynamics (Equation 1) can be written in terms of Equation 3 as:

$$M(q_c)\ddot{q}^d_c - M(q_c)\ddot{e} + N(q_c, \dot{q}_c) = \frac{r+1}{r}\tau_h. \tag{4}$$

In state-space form, Equation 4 can be written as:

$$\dot{\mathbf{e}} = A_0\mathbf{e} + B_0[\ddot{q}^d_c + M^{-1}N - M^{-1}\frac{r+1}{r}\tau_h], \tag{5}$$

where:

$$A_0 = \begin{bmatrix} 0 & I \\ 0 & 0 \end{bmatrix}, \quad B_0 = \begin{bmatrix} 0 \\ I \end{bmatrix}, \quad \mathbf{e} = \begin{bmatrix} e \\ \dot{e} \end{bmatrix}. \tag{6}$$

Since there is no exogenous input in Equation 5, let $B_0M^{-1}u_l$ on the RHS of Equation 5 be added and subtracted to yield:

$$\dot{\mathbf{e}} = A_0\mathbf{e} + B_0[\ddot{q}^d_c + M^{-1}N - M^{-1}u_l] + B_0M^{-1}[u_l - \frac{r+1}{r}\tau_h], \tag{7}$$

where u_l is a $n \times 1$ vector of a virtual control input to be defined later. It is assumed that u_l can be designed so that the tracking error $\mathbf{e}$ approaches zero in spite of external disturbances. Herein, u_l is chosen as:

$$u_l = \hat{M}(\ddot{q}^d_c - u_\infty) + \hat{N}, \tag{8}$$

where $\hat{M}$ and $\hat{N}$ are the mathematical models of the M and N, respectively, and u_∞ is the new control input, designed using $\mathcal{H}_\infty-$ and μ-synthesis design methods. Substituting Equation 8 for only the first u_l in RHS of Equation 8 yields:

$$\dot{\mathbf{e}} = A_0\mathbf{e} + B_0(\eta + u_\infty) + B_0M^{-1}[u_l - \frac{r+1}{r}\tau_h], \tag{9}$$

where:

$$\eta = \Delta(\ddot{q}^d_c + u_\infty) + \delta$$

$$\Delta = I - M^{-1}\hat{M}, \quad \delta = M^{-1}(N - \hat{N}),$$

let one define:

$$\eta_{\mathbf{f}} = [u_l - \frac{r+1}{r}\tau_h], \tag{10}$$

then, one can write Equation 9 as:

$$\dot{\mathbf{e}} = A_0\mathbf{e} + B_0(\eta + u_\infty) + B_0M^{-1}C\eta_{\mathbf{f}}, \tag{11}$$

where:

$$C = [I \quad 0], \quad \eta_{\mathbf{f}} = \begin{bmatrix} \eta_{\mathbf{f}} \\ \dot{\eta}_{\mathbf{f}} \end{bmatrix} = \begin{bmatrix} u_l - \frac{r+1}{r}\tau_h \\ \dot{u}_l - \frac{r+1}{r}\dot{\tau}_h \end{bmatrix}. \tag{12}$$

In Equation 11 if the last term ($\eta_{\mathbf{f}}$) is made to vanish, then it reduces to a usual state-space error equation where, by appropriate design of u_∞, the error would stably vanish. Hence, the goal is to force $\eta_{\mathbf{f}}$ to zero. This requirement can be satisfied if the dynamics of the actuator and transmission system is known. In other words, an actuator-level torque control law has to be designed to provide the desired torque, based on Equation 8. Furthermore, having the following procedure for control design, it is required that the actuator-level

torque characteristic of the joint is identified, which is explained in the next section.

Next section presents the experimental identification of the actuator-transmission system models. Moreover, the determination of uncertainty bounds to incorporate the effect of the variations between the real system and the identified model is introduced. Finally, an actuator-level robust $\mathcal{H}_\infty-$ based torque controller is designed to guarantee the stability and convergence of the error dynamics.

EXPERIMENTAL IDENTIFICATION OF THE TORQUE TRANSFER FUNCTION

The frequency response method is used to experimentally provide an input-output torque model of the IRIS-facility test-joint. Such experiments can be dangerous if the arm is unrestrained, due to the elastic coupling between high-frequency "internal" (joint) and low-frequency "external" (arm) dynamics. In contrast, the experiments can be performed successfully if the arm is restrained against a stiff environment. The stiff environment prevents the external dynamics from being excited, such that no effect on the internal dynamics takes place. The experiments were carried out for the test-joint using an input signal frequency in the range of 0-150 Hz. The same set of experiments were repeated for varying levels of input signal amplitude. Figures 1 and 2 show the magnitude and phase plots of input-output torque ($\frac{\tau_h}{\tau_m}$) for three different amplitudes of sinusoidal signal.

Since the highest useful frequency of the system is below 100 Hz, the transfer function of the input-output torque is based on the experimental data in the range of 0-100Hz. More precise analysis using Signal Processing and Identification Toolbox of MATLAB [15] shows that the transfer function can be approximated

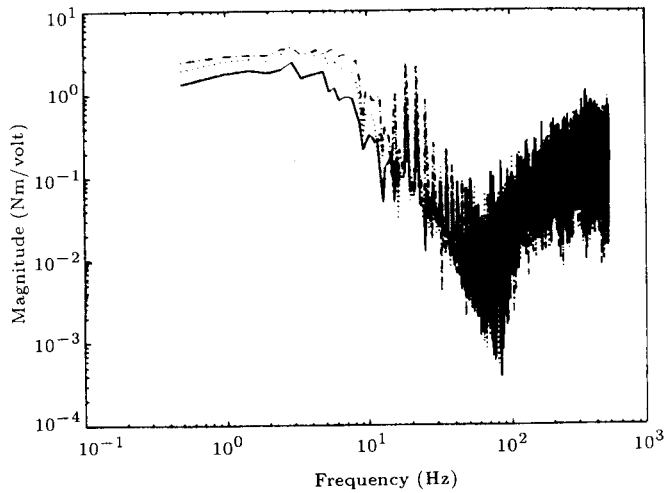

Figure 1. Input-output torque magnitude plot of IRIS-joint for three different input signal amplitude.

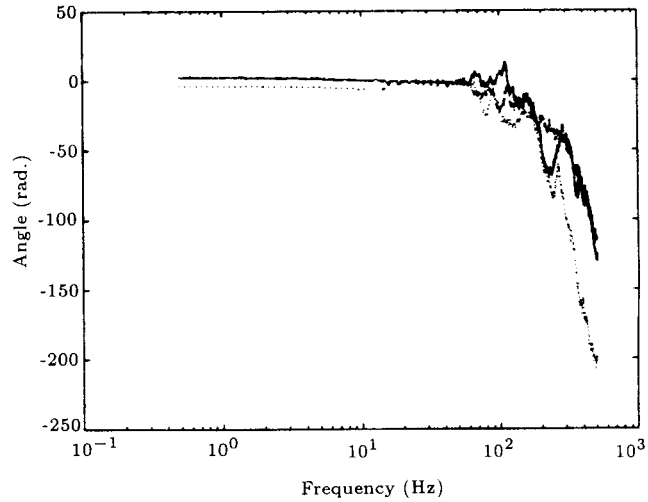

Figure 2. Input-output torque phase plots of IRIS-joint for three different input signal amplitude.

by $P_{\text{nom}}(s) = \frac{b(s)}{a(s)}$, where $b(s)$ and $a(s)$ are second and fourth order polynomials, respectively, given as:

$$b(s) = 0.001 * (-0.0022s^2 - 0.1411s + 0.1258), \tag{13}$$

$$a(s) = s^4 - 3.9607s^3 + 5.9049s^2 - 3.9276s + 0.9834. \tag{14}$$

Comparison of the measured and identified input-output torque signals in Figure 3 shows a very good match for the operating range of 0-100Hz.

The variations between the measured and identified torque transfer function are modeled as uncertainty bounds in the proposed control design method. A robust $\mathcal{H}_\infty-$ design approach is proposed to incorporate these variations and to guarantee the robustness and performance of the closed-loop system. The selection of uncertainty descriptions and bounds is described in more detail in the next section.

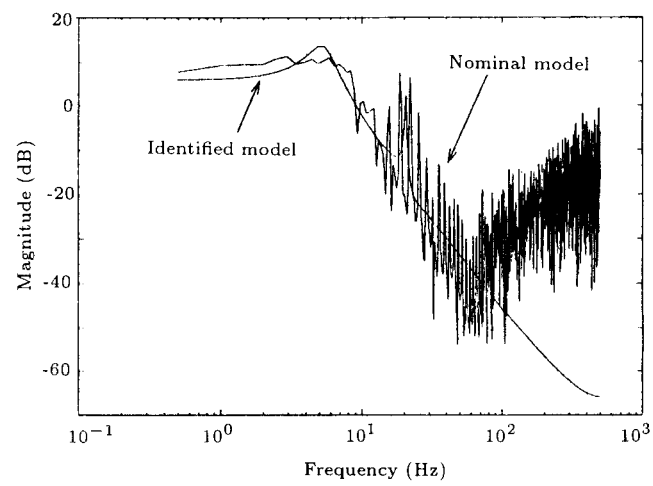

Figure 3. Measured and identified input-output torque transfer function of the IRIS-joint.

DETERMINATION OF UNCERTAINTY BOUNDS

A frequency domain uncertainty description is employed to account for the variation between the measured and identified models. A multiplicative uncertainty weight is used to account for the low frequency inaccuracies (below 0.2 Hz) and the unmodeled high frequency dynamics (above 50 Hz). It is modeled as an unstructured full block uncertainty, Δ_1, located before the error dynamics transfer matrix (P_{nom}) (Figure 4). The magnitude of the multiplicative uncertainty weight at high frequency is selected to envelope the unmodeled modes of the system. A plot of the worst case variations between the measured and identified models, along with the multiplicative uncertainty weight, are shown in Figure 5. Moreover, an additive uncertainty weight, W_n, is included to represent the torque sensor noise measurement (Figure 5). It envelopes the torque sensor noise characteristics in the frequency range of its application. Also, to limit the actuator power in control design, W_a has been considered, which models the servo motor characteristic used in this robot. To reflect the various performance requirements in different frequency ranges, another weighting matrix is included (W_p). The set of weighting functions that are used for the test-joint control design purposes are as follows:

1. Model uncertainty weight:

$$W_{\text{mult}}(s) = r.\frac{500s + 5000}{s + 10000}, \tag{15}$$

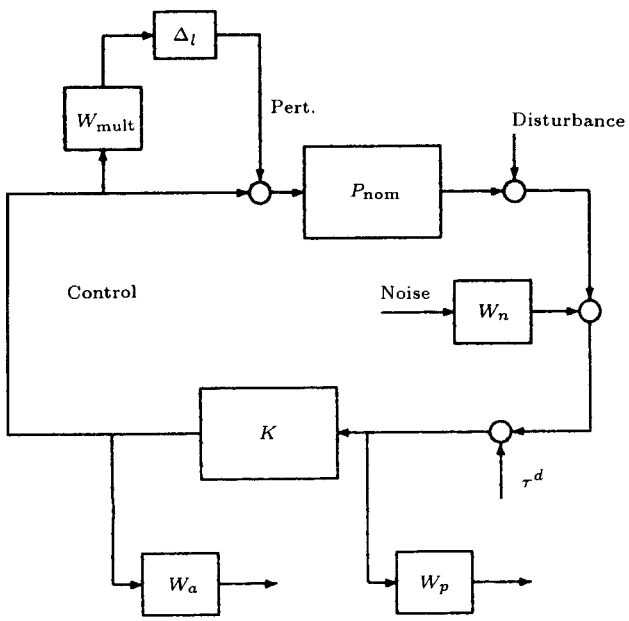

Figure 4. Block diagram of trade-off control problem formulation.

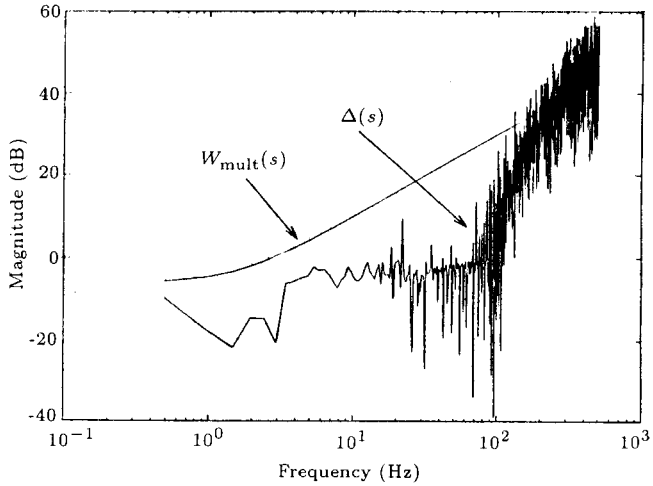

Figure 5. Magnitude plot of error torque and multiplicative uncertainty weight.

2. Noise weight:

$$W_n(s) = n.\frac{2s + 2.56}{s + 320}, \tag{16}$$

3. Performance weight:

$$W_p(s) = p.\frac{0.005s + 200}{0.01s + 0.00518}, \tag{17}$$

4. Actuator saturation weight:

$$W_a(s) = a.\frac{0.01s + 0.01}{0.01s + 0.001}. \tag{18}$$

where the unknown parameters (r, n, p, a) are selected based on performance and robustness requirements in the control design method.

TORQUE CONTROL DESIGN

In the previous section, uncertainty descriptions are introduced to account for variations between models and the physical system. The selection of uncertainty descriptions plays a major role in the trade-off between robustness and performance requirements in the control design process.

This section investigates this trade-off in the selection of uncertainty descriptions and levels for the test-joint experiment. The control objective is to track a desired command torque in spite of nonlinearities, friction and flexibility in the actuator-transmission system. This is formulated as minimizing the $\|.\|_\infty$ norm between the input disturbances and sensor outputs. Moreover, the block diagram is reformulated into the Linear Fractional Transformation (LFT) framework to design control laws using the μ-synthesis methodology (Figure 6). The dimensions of the Δ blocks are: 1×1 for Δ_1, and 3×2 for Δ_2. Δ_1 is associated

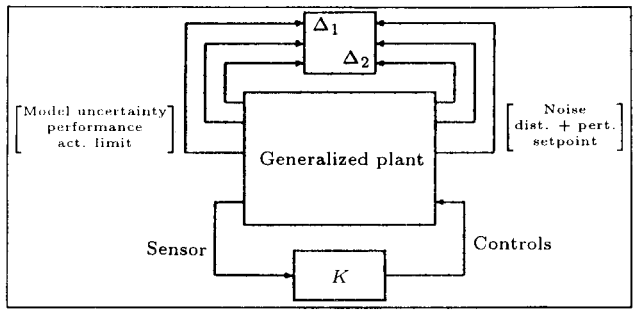

Figure 6. LFT of trade-off control problem formulation.

with the multiplicative uncertainty and Δ_2 with the performance specification weights (i.e. W_a, W_p).

Different control laws are designed for the test-joint experiment by varying the levels of uncertainty weights. A set of controllers is designed by varying the multiplicative uncertainty weight bound and keeping the rest of weighting functions fixed. Another set of controllers is designed by varying the actuator-saturation level weight while keeping the multiplicative uncertainty weight fixed. For further details, the reader may refer to [16].

EXPERIMENTAL SETUP FACILITY

This section briefly presents the IRIS-facility experimental setup introduced in [13,17] (Figure 7). The IRIS-facility is a versatile and reconfigurable robot arm. It is designed to be easily disassembled and assembled as required and provides a multitude of configurations. Each joint-module is composed of a frameless DC-motor, HD gear, an optical rotary encoder to measure the motor displacement and a custom-designed torque sensor to measure the load torque.

For the purpose of experimental tests, the joint-module is constituted of a RBE-01202 motor (Inland Motor Corp.) capable of delivering up to 1.12 Nm. The motor is coupled to a harmonic drive with 100:1 speed reduction [18]. The rated torque of this unit is 40 Nm,

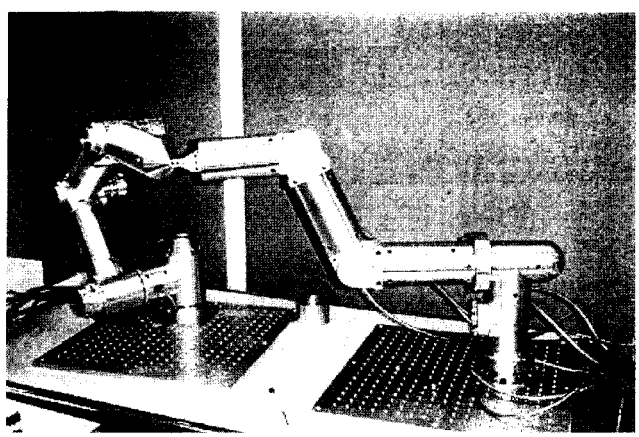

Figure 7. IRIS arms.

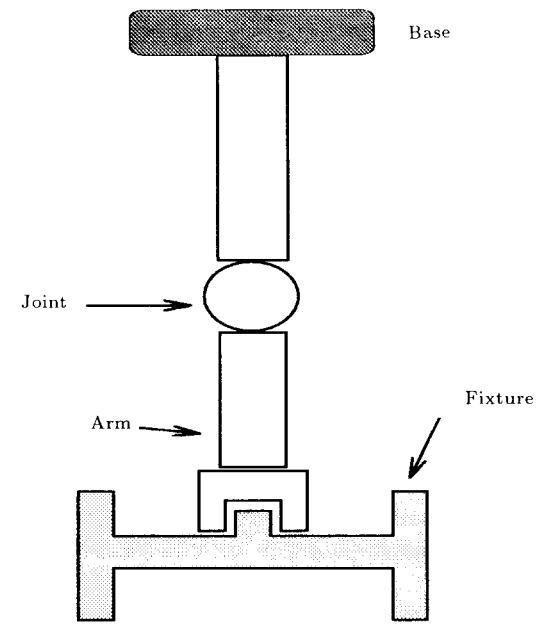

Figure 8. Restrained motion setup.

maximum average torque is 49 Nm and momentary peak torque is 108.4 Nm. A custom-designed torque sensor, which has a stiffness coefficient 10 times higher than that of the harmonic drive, is used to measure the load torque.

For the purpose of torque-feedback control design, the stator of the joint-test motor is fixed to a stationary frame. Hence, the measured torque is proportional to the torque experienced by the rotor (Figure 8).

EXPERIMENTAL RESULTS

Model Uncertainty Weight Variation

Three control laws are synthesized based on the block diagram in Figure 4, with varying levels of model uncertainty weight (i.e. W_{mult} varied), while the rest of the weighting functions are kept constant. Table 1 contains a list of the control parameters used in the design and the results of implementation on the test-joint experiment. The parameters in the table are from Equations 15 to 18.

The closed-loop torque responses of the test-joint experiment for implementing these controllers are shown in Figures 9 to 14. MU-K1 achieves a μ value

Table 1. Parameters for control design with fixed performance weight.

Ctrl.	Input	a	n	p	r	μ	Figure
MU-K1	Step	1.0	10^{-4}	10^{-3}	0.01	9.4	Figure 9
MU-K2	Step	1.0	10^{-4}	10^{-3}	0.1	1.3	Figure 10
MU-K3	Step	1.0	10^{-4}	10^{-3}	1.0	2.7	Figure 11
MU-K1	Sin	1.0	10^{-4}	10^{-3}	0.01	9.4	Figure 12
MU-K2	Sin	1.0	10^{-4}	10^{-3}	0.1	1.3	Fiure 13
MU-K3	Sin	1.0	10^{-4}	10^{-3}	1.0	2.7	Figure 14

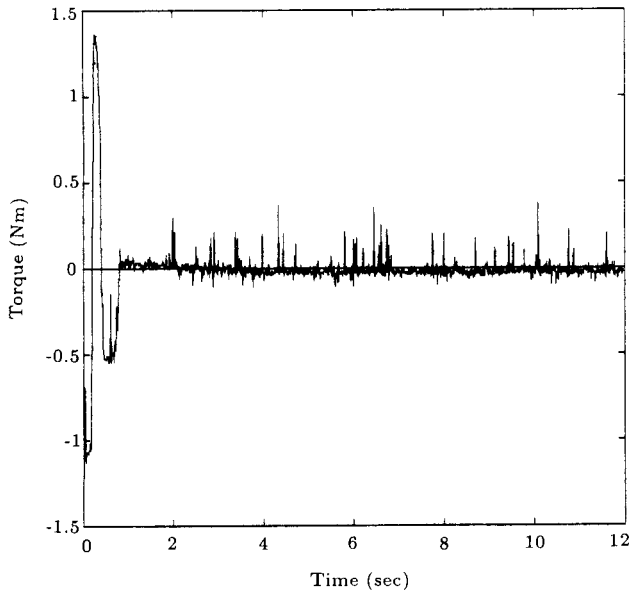

Figure 9. Step response of the IRIS-joint for controller MU-K1.

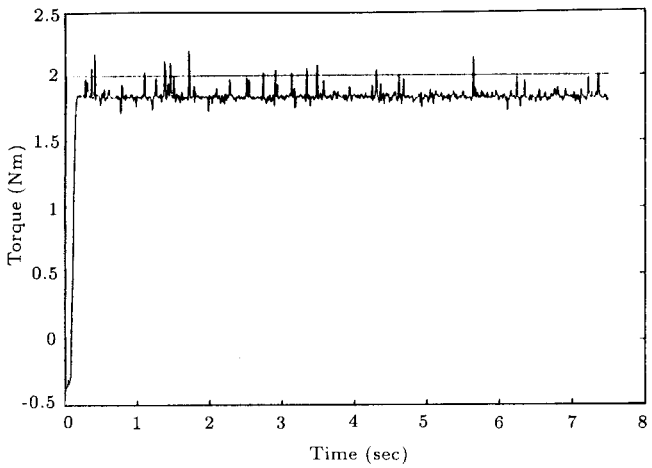

Figure 10. Step response of the IRIS-joint for controller MU-K2.

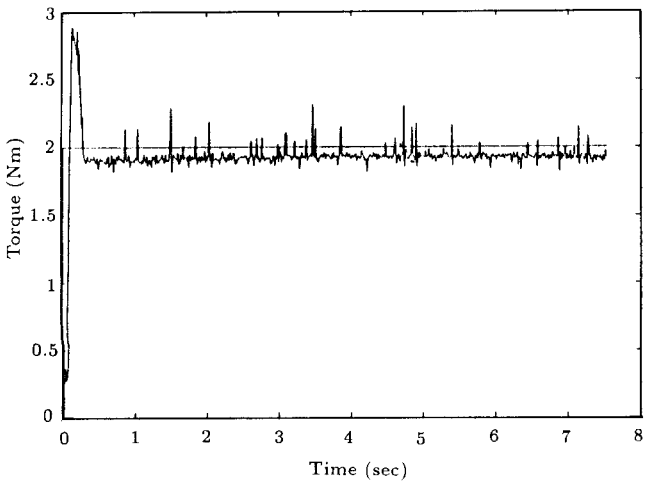

Figure 11. Step response of the IRIS-joint for controller MU-K3.

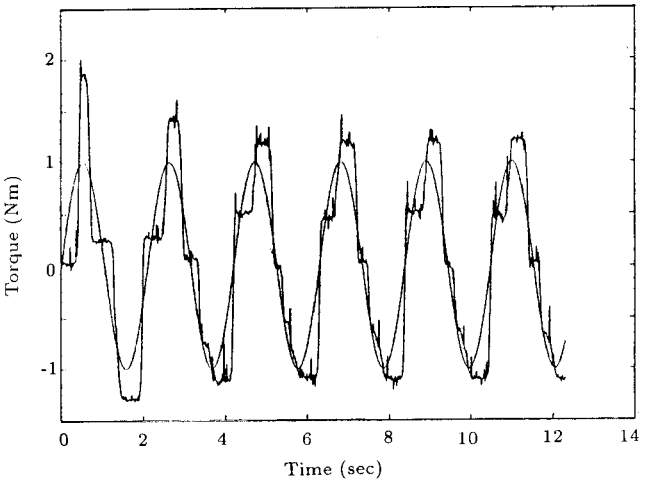

Figure 12. Sinusoidal response of the IRIS-joint for controller MU-K1.

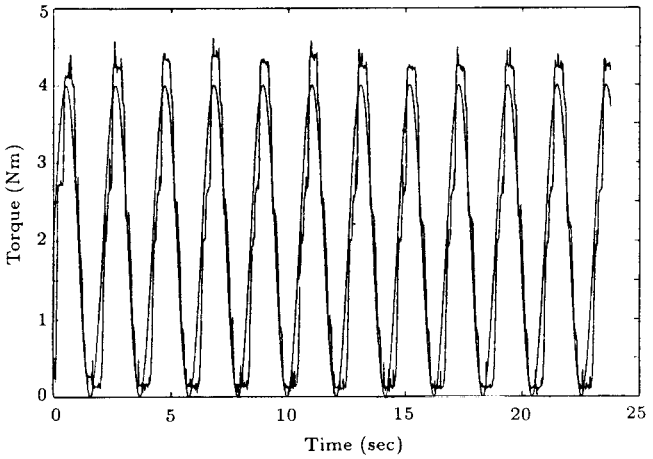

Figure 13. Sinusoidal response of the IRIS-joint for controller MU-K2.

of 9.4 and the step response settles down in about 1 second. However, the step response shows an overshoot as high as two times the desired step command. MU-K2 is designed by increasing the model uncertainty weight by a factor of 10 compared to the previous case. However, the step response does not show any overshoot, but a steady-state error of 15% can be observed (Figure 10). The level of uncertainty weight is increased to 1 in the MU-K3 controller and it can be observed that the step response of the system is better compared to the two previous cases.

Figures 12 to 14 show the sinusoidal response of the system for the same sets of controllers. In this set of experiments, controller MU-K3 shows superior performance compared to the two other controllers.

Actuator-Saturation Limit

A series of control laws is synthesized using varying levels of actuator-saturation limits (i.e., W_a is varied),

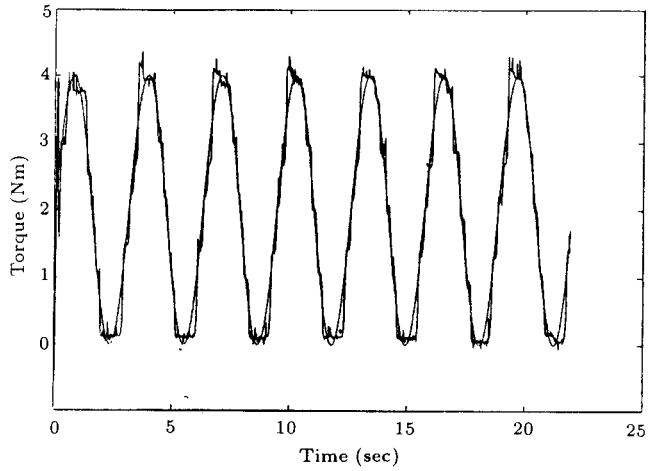

Figure 14. Sinusoidal response of the IRIS-joint for controller MU-K3.

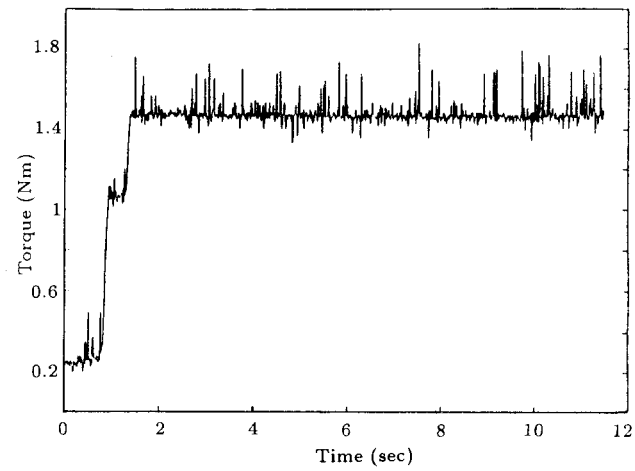

Figure 16. Step response of the IRIS-joint for controller AC-K2.

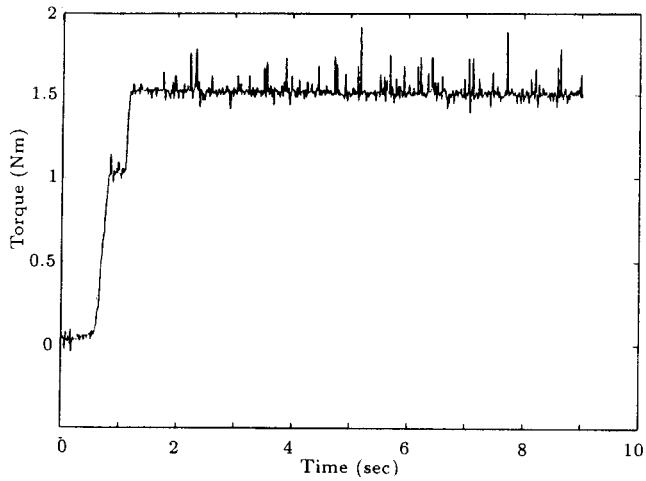

Figure 15. Step response of the IRIS-joint for controller AC-K1.

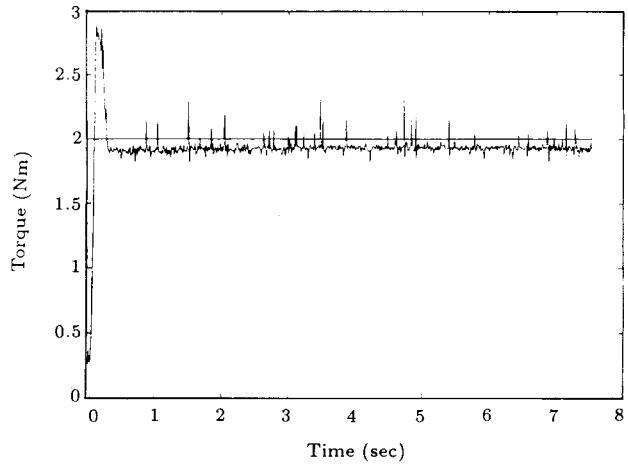

Figure 17. Step response of the IRIS-joint for controller AC-K3.

while multiplicative uncertainty and noise weights remain fixed. Table 2 shows the control parameters used in the design and the results of implementation on the test-joint experiment.

Figure 15 shows the step torque responses of the test-joint for controller AC-K1. The actuator-saturation level is chosen as 10 in this case. If the actuator-saturation limit is decreased to 2 (i.e. AC-K2 controller), the performance of the system does not change compared to the first case (Figure 16). But if the actuator-saturation limit is decreased to 1, the steady-state error gets smaller values (Figure 17). Figures 18 to 20 show a set of sinusoidal responses

Table 2. Parameters for control design with varying performance weight.

Crtl.	Input	a	n	p	r	μ	Figure
AC-K1	Step	10.0	10^{-4}	10^{-5}	1.0	2.26	Figure 15
AC-K2	Step	2.0	10^{-4}	10^{-3}	1.0	2.27	Figure 16
AC-K3	Step	1.0	10^{-4}	10^{-3}	1.0	2.7	Figure 17

Table 3. Parameters for control design with varying performance and uncertainty weight.

Crtl.	Input	a	n	p	r	μ	Figure
AC-K4	Sin	2.0	10^{-4}	10^{-3}	10^{-3}	1.55	Figure 18
AC-K5	Sin	1.0	10^{-4}	10^{-3}	0.01	9.4	Figure 19
AC-K6	Sin	0.5	10^{-4}	10^{-3}	0.001	0.73	Figure 20

of the system for varying actuator-saturation limits and model uncertainty weights, simultaneously. The controller AC-K4, with a saturation level of 2 and model uncertainty weight of 0.001, achieves the best performance in comparison to the two other cases (Table 3).

CONCLUSIONS

Representing the actuator-transmission system in flexible joint robots with a nominal model and an uncertainty description provides an excellent model for use in robust torque control design. The theoretical

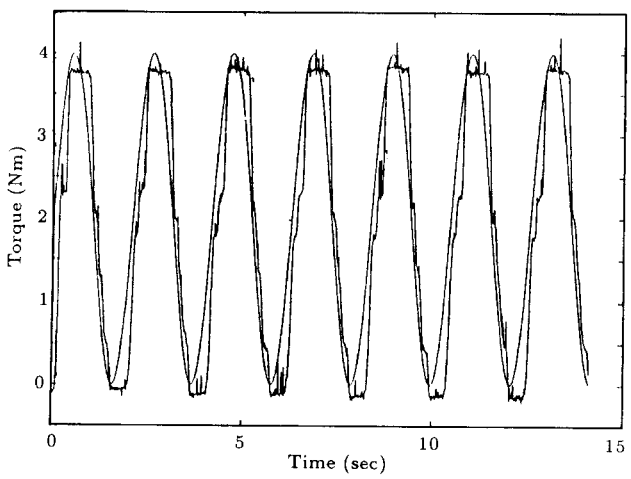

Figure 18. Sinusoidal response of the IRIS-joint for controller AC-K4.

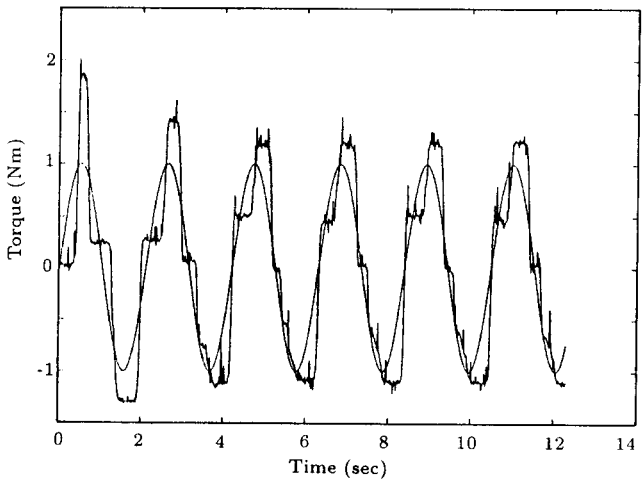

Figure 19. Sinusoidal response of the IRIS-joint for controller AC-K5.

and experimental results indicate that uncertainty modeling plays a major role in the trade-off between performance requirements and robustness properties of synthesized control laws. A series of control laws are synthesized with a varying level of model uncertainty and actuator-saturation limit. It is experimentally verified that the performance of the system is sensitive to the uncertainty description and the actuator-saturation level in the control design. Increasing the level of the multiplicative uncertainty model while the actuator-saturation level is fixed, leads to a better performance of the system. On the other hand, choosing a high level of actuator-saturation limit, while the model uncertainty weight remains fixed, deteriorates the performance and large steady-state errors appear in the step response. Furthermore, it is verified that varying, simultaneously, the performance and model uncertainty weights, leads to high performance closed-loop systems.

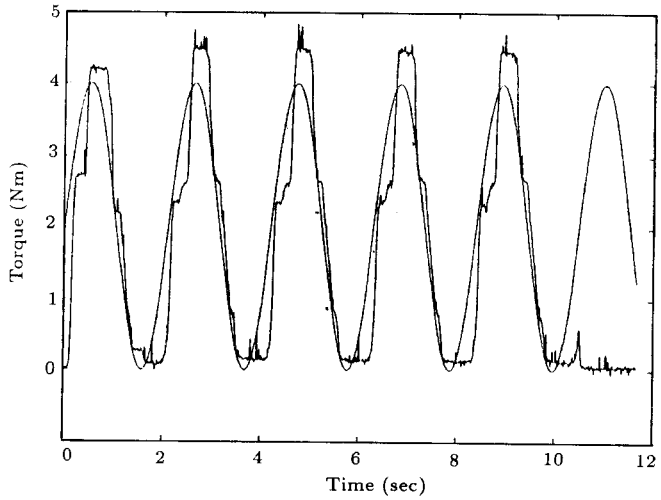

Figure 20. Sinusoidal response of the IRIS-joint for controller AC-K6.

REFERENCES

1. Asada, H., Youcef-Toumi, K. and Lim, S.K. "Joint torque measurement of a direct drive arm", *Proceedings of IEEE Conference on Decision and Control*, pp 1332-1337 (1984).
2. Riven, E., *Mechanical Design of Robots*, McGraw-Hill (1988).
3. Sweet, L.M. and Good, M.C. "Redefinition of the robot motion-control problem", *IEEE Control Systems Magazine*, pp 18-25 (Aug. 1985).
4. Tomei, P. "A simple PD controller for robots with elastic joints", *IEEE Transactions on Automatic Control*, **36**(10), pp 1208-1213 (Oct. 1991).
5. Marino, R. and Nicosia, S. "On the control of robots with elastic joints", *Proceedings of the American Control Conference*, pp 69-70 (1985).
6. Al-Ashoor, R.A., Khorasani, K., Patel, R.V. and Al-Khalili, A.J. "Robust adaptive controller design for flexible joint manipulators", *Robotics and Computer-Integrated Manufacturing*, **9**(2), pp 101-112 (April 1992).
7. Spong, M.W. "Modeling and control of flexible joint manipulators", *Journal of Dynamic Systems, Measurements and Control*, **109**, pp 310-319 (1987).
8. Hashimoto, M., Horiuchi, T., Kiyosawa, Y. and Hirabayashi, H. "The effects of joint flexibility on robot motion control based on joint torque positive feedback", *Proceedings of IEEE International Conference on Robotics and Automation*, pp 1220-1225 (April 1991).
9. Tian Lin and Goldenberg, A.A. "Robust adaptive control of flexible joint robots with joint torque feedback", *Proceedings of IEEE International Conference on Robotics and Automation*, pp 1229-1234 (1996).
10. Moghaddam, M.M. and Goldenberg, A.A. "Robustness and performance trade-offs in torque control of robots with armonic drive transmission", *Proceedings of the*

IEEE International Conference on Robotics and Automation, pp 2365-2370 (April 1997).

11. Kanellakppoulos, I., Kokotovic, P.V. and Morse, A.S. "Systematic design of adaptive controllers for feedback linearizable systems", *IEEE Transactions on Automatic Control*, **36**, pp 1241-53 (1991).

12. Qu, Z. "Globally stable i/o robust control of flexible joint robots", *Proceedings of IEEE International Conference on Robotics and Automation*, **3**, pp 1004-1010 (1993).

13. Kircanski, N., Goldenberg, A.A. and Jia, S. "An experimental study of nonlinear stiffness, hysteresis, and friction effects in robot joint with harmonic drives and torque sensors", *Proceedings of the 3rd International Symposium on Experimental Robotics*, **1**, pp 147-154 (1993).

14. Moghaddam, M.M. and Goldenberg, A.A. "Nonlinear modeling and robust $\mathcal{H}_\infty$- based control of flexible joint robots with harmonic drives", *Proceedings of the IEEE International Conference on Robotics and Automation*, pp 3130-3135 (April 1997).

15. MATHWorks Inc. *A Program for Simulating Dynamic Systems*, User's Guide, The MATH Works Inc. (1992).

16. Moghaddam, M.M., *Robust $\mathcal{H}_\infty-$ Based Control of Flexible Joint Robots with Harmonic Drive Transmission*, PhD thesis, University of Toronto, Toronto, Ontario, Canada (Feb. 1997).

17. Kircanski, N. "Iris grasping and manipulation facility", *Proceedings of IEEE International Conference on Robotics and Automation*, **3**, 155-160 (1993).

18. Harmonic Drive Gearing, *CUP Type HDUC and HIUC Component Sets*, HD Systems Inc., New York, USA.